https://doi.org/10.52676/1729-7885-2026-2-37-46
УДК 538.9

# REVIEW: OPTICAL PROPERTIES OF SILICON CARBIDE-BASED COMPOSITE MATERIALS

**S. N. Hamidova*, V. U. Mammadov**

***Baku State University, Baku, Azerbaijan***

** E-mail for contacts: hamidova.sevinc.natiq@bsu.edu.az*

This review provides a comprehensive analysis of the optical properties of silicon carbide (SiC) across various structural forms, from bulk crystals to 0D nanostructures and depending on different parameters and factors. The study systematically evaluates the dependence of SiC's intrinsic optical response on its polytypism, where the indirect band gap is shown to scale with hexagonality from 2.36 eV (3C-SiC) to 3.23 eV (4H-SiC). For thin films and heterostructures, it is observed that processing parameters, such as annealing at 800°C and increasing layer thickness to 250 nm, optimize crystallinity and reduce the absorption coefficient by nearly 20%. At the nanoscale, quantum confinement effects induce a significant blue shift in optical transitions, with band gaps reaching 4.5 eV in 0D quantum dots. The review further details the impact of excitonic binding energies, which reach values of 0.5–1.0 eV in 2D SiC monolayers, highlighting the necessity of GW+BSE many-body corrections for accurate optical modeling over standard DFT methods. Finally, the investigation of SiC nanofluids reveals a 150% enhancement in solar absorption efficiency and 98% long-term durability, confirming SiC as a robust candidate for direct absorption solar collectors. The work concludes by identifying current gaps between theoretical predictions and experimental validation, emphasizing the need for integrated modeling in future SiC-based photonic research.

***Keywords:*** *SiC, optical properties, band gap value, polytypism, quantum confinement, excitonic effects, thin films, nanofluids, solar absorption.*

## 1. Introduction

Silicon carbide (SiC) is a wide-bandgap semiconductor valued for its exceptional optical, electronic, thermal, and mechanical properties [1, 2]. Its high thermal conductivity, chemical stability, and radiation hardness make it a cornerstone material for high-power electronics, harsh-environment photonics, and emerging quantum technologies [3–5]. Recent advances have enabled SiC synthesis from renewable precursors, such as rice husk, offering sustainable production routes [6]. Beyond photonics, SiC-based materials also show promise as electrodes for high-performance supercapacitors [7].

A defining feature of SiC is its rich polytypism, with over 200 known polytypes (primarily 3C, 4H, and 6H) [8, 9]. Variations in stacking sequences lead to distinct electronic band structures and optical responses. Extensive studies using spectroscopic ellipsometry and first-principles calculations have clarified the role of crystallographic structure, temperature, and surface treatment on the optical constants of bulk SiC [2, 10, 11]. Similarly, the optical properties of SiC thin films and heterostructures are highly sensitive to deposition methods, annealing conditions, and interface effects, which allow for precise tuning of refractive index and absorption [12–18].

At the nanoscale, low-dimensional structures (nanosheets, nanowires, and quantum dots) exhibit properties governed by quantum confinement and surface effects [19, 20]. These phenomena, which include tunable band gaps and pronounced excitonic effects, are typically elucidated through many-body approaches like GW and the Bethe–Salpeter equation [21-23]. Concurrently, optically active defects and color centers (e.g., divacancies and vanadium impurities) have positioned SiC as a leading platform for quantum sensing and room-temperature qubits [4, 5]. Notably, vanadium defects in 4H-SiC provide emission in the telecommunication O-band (1.28–1.33 μm), enabling direct integration with fiber-optic networks [24]. Additionally, SiC nanoparticles in nanofluids significantly enhance solar–thermal conversion efficiency, extending the material's utility to renewable energy technologies [25-27].

While SiC optics are often discussed in fragmented contexts, this review provides an integrated analysis across all material scales – from bulk crystals and thin films to 2D nanostructures and defect-engineered systems. By synthesizing experimental data and theoretical insights, this work identifies current research gaps and highlights future directions for SiC-based optical materials.

## 2. Band structure dependence on different factors

### *2.1. Dependence on the polytypes of SiC*

The intrinsic optical properties of bulk SiC are fundamentally governed by its polytypism, crystallographic order, and electronic band structure. A systematic understanding of these properties is essential, as bulk SiC serves both as a reference material for thin films and nanostructures and as a functional optical medium in its own right.

A comprehensive perspective on the relationship between SiC polytypism and optical transitions is provided in [8]. The study highlights that variations in the stacking sequence of Si-C bilayers – cubic for 3C and hexagonal for 4H and 6H – lead to distinct electronic structures. Specifically, the indirect band gap increases with the degree of hexagonality: from 2.36 eV for 3C-SiC (0% hexagonality) to 3.02 eV for 6H-SiC (33% hex.) and reaching 3.23 eV for 4H-SiC (50% hex.) [8, 10]. This shift occurs because the change in the stacking order modifies the crystal potential and the Brillouin zone folding, which shifts the conduction band minima, thereby widening the energy gap as the structure becomes more hexagonal.

Experimental determination of optical constants by Zhang et al. [2] provides quantitative data on the refractive index and extinction coefficient. At a standard wavelength of 633 nm, the refractive index varies between 2.55 for 3C-SiC and approximately 2.65–2.69 for the hexagonal polytypes (4H and 6H) [2, 9]. The higher refractive index in hexagonal polytypes is attributed to the increased density and the anisotropic nature of the hexagonal lattice, which leads to a more compact electronic distribution compared to the cubic 3C-SiC structure.

First-principles calculations by Montañez et al. [9] offer a systematic comparison of the dielectric response. Their results quantify the high-frequency dielectric constant (n), showing values of ~6.52 for 3C-SiC, while for 4H and 6H, these values are slightly lower (~6.3–6.4) due to the influence of crystalline anisotropy. The study explains that in 4H-SiC and 6H-SiC, the presence of birefringence (the difference between ordinary and extraordinary indices) is a direct consequence of the lower symmetry of the hexagonal crystal system compared to the cubic system.

Comparing the results of experimental [2] and first-principles theoretical [9, 10] studies, it can be concluded that the optical response of SiC is strongly governed by its hexagonality. As the polytype shifts from 3C to 4H, the band gap increases by approximately 0.87 eV, significantly shifting the optical absorption edge toward the ultraviolet region. It should be noted, however, that this relationship is monotonic rather than strictly linear: the rate of band gap increase with hexagonality is not constant across all polytypes, because the conduction band minimum (CBM) shifts between different symmetry points in the Brillouin zone (from X in 3C to M and K in 4H and 6H) as the stacking sequence changes. This CBM repositioning modifies the indirect transition energy non-uniformly, so the 3C→6H step and the 6H→4H step produce different band gap increments despite a nominally linear hexagonality scale [8, 9]. While theoretical models provide idealized values, experimental data show that surface conditions and defects in bulk 6H-SiC can lower the observed transmittance by 5–10% compared to theoretical predictions. Thus, for high-precision optoelectronics, 4H-SiC is preferred for UV applications due to its wider gap, while 3C-SiC is more suitable for integration with Si due to its lower lattice mismatch and smaller energy gap.

### *2.2. Dependence on different technical parameters*

The reliability of optical data for SiC depends significantly on the measurement methodology and external physical conditions. Kunle et al. [28] performed a comparative optical characterization of bulk SiC, demonstrating that the choice of technique (e.g., UV-Vis spectroscopy vs. spectroscopic ellipsometry) affects the extracted parameters. For instance, the absorption coefficient (alpha) can show variations of up to 10-15% depending on whether reflectance or transmittance geometry is used. At a wavelength of 500 nm, the absorption coefficient was measured to be approximately 100-150 cm^-1. This discrepancy is attributed to surface roughness and the presence of a thin native oxide layer (typically 2-5 nm thick), which complicates the extraction of intrinsic bulk constants [28].

Temperature-dependent optical behavior is a critical factor for SiC applications. Zhang and Kioupakis [10] calculated the temperature-dependent optical absorption spectra of 3C, 4H, and 6H-SiC polytypes using first-principles methods, demonstrating a consistent redshift (narrowing) of the band gap as temperature increases. For 6H-SiC, the band gap $E_g$ decreased from 3.02 eV at 300 K to approximately 2.91 eV at 600 K. For 4H-SiC, the value dropped from 3.23 eV to 3.11 eV in the same range [10]. This behavior is explained by the Varshni effect, where increasing temperature leads to lattice expansion and an increase in electron-phonon interactions, which effectively shifts the energy levels of the valence and conduction bands closer together.

Refined experimental datasets for bulk SiC were recently presented by Kar et al. [29]. This work focuses on the dispersion of the refractive index (n) across the visible and near-infrared regions (400-1000 nm). The researchers reported that for high-purity 6H-SiC, the refractive index follows a Cauchy-like dispersion, with values decreasing from 2.72 at 400 nm to 2.58 at 800 nm [29]. These high-precision constants are essential for modeling photonic structures, as the study shows that even a 1% change in stoichiometry can shift the refractive index by approximately 0.02, affecting the optical path length in devices.

Regarding thin-film systems, Larruquert et al. [1] provided reference-quality data using spectroscopic ellipsometry. Their study determined that the optical constants of SiC films are highly sensitive to the photon energy in the range of 1.5 to 5.0 eV. For films deposited at room temperature, the refractive index (n) at 633 nm was found to be approximately 2.45-2.48, which is 5-7% lower than the bulk value (around 2.65) due to lower packing density and the presence of amorphous phases [1]. The study identifies that the extinction coefficient (k) remains low (under 0.01) in the visible range but

increases significantly in the UV region (above 3.5 eV), reaching values over 0.6, which is directly related to the high density of dangling bonds and structural disorder in the thin-film matrix [1].

The comparison of these studies [1, 10, 28, 29] reveals that SiC optical parameters are highly sensitive to external factors. The band gap narrows at a rate of approximately 0.38–0.45 meV/K, and the refractive index of thin films is consistently lower than bulk values by about 0.2. These specific values must be used when designing SiC-based components: the temperature-corrected band gap from [10] is vital for high-heat sensors, while the dispersion data from [29] is necessary for high-precision optical coatings.

***2.3. Influence of processing parameters: Thickness, Annealing, and Deposition***

The optical response of SiC thin films is highly sensitive to processing conditions. Thermal annealing at 400–800°C [12] reduces the absorption coefficient (alpha) by nearly 20% at 800°C due to structural ordering and reduced defect density. Film thickness also dictates optical behavior [13]: for 50 nm films, alpha ~2.5*$10^4$ $cm^{-1}$, decreasing to 1.8 *$10^4$ $cm^{-1}$ at 250 nm as grain size and crystallinity improve as shown in Figure below. Ellipsometric data [11] show that the refractive index (n) at 600 nm rises from 2.15 to 2.40 with increasing film density. A 10–12% variation in $n$ between studies [1, 11] is attributed to substrate temperature, where higher temperatures facilitate a more compact lattice and higher electronic polarizability. Deposition time also influences the bandgap; increasing growth from 30 to 90 minutes [14] shifts $E_g$ from 2.1 eV to 2.35 eV. This "blue shift" results from reduced disorder (Urbach tail energy), whereas shorter growth times lead to higher extinction coefficients (k) due to incomplete Si-C bonding. Synthesized data [11-14] suggest that thermal annealing is the most effective way to increase transparency, while thickness and deposition time improve crystallinity and increase $E_g$ by ~0.25 eV. For high-precision optics, films >200 nm annealed at 800°C are recommended to achieve n ~2.4–2.5. Furthermore, PVD-deposited films [30] exhibit fewer Si–H and C–H defects than CVD counterparts, resulting in lower extinction coefficients (k < 0.005) in the visible range. Consequently, PVD serves as a primary route for high transparency when high-temperature annealing is not feasible [12, 14, 30].

***2.4. Surface treatment, oxidation, and implantation effects on the optical properties***

Beyond intrinsic material properties and thin-film growth parameters, the optical response of SiC is strongly influenced by surface modification processes and defect engineering. Shi et al. [3] investigated the effects of surface treatment on 4H-SiC thin films for integrated photonics, demonstrating that chemical-mechanical polishing can reduce the surface roughness from 3.67 nm to 0.15 nm, which leads to a significant reduction in light scattering loss and an increase in reflectance by approximately 8-12% in the UV region (200-400 nm). This improvement occurs because the removal of the damaged surface layer eliminates parasitic light scattering and surface-localized states that otherwise act as absorption centers. Oxidation-induced optical changes were examined by Charpentier et al. [15] in Si-SiC composites. The study analyzed how the formation of a silica (SiO2) surface layer affects the overall reflectance. Their findings show that for an oxide layer thickness of approximately 20-50 nm, the

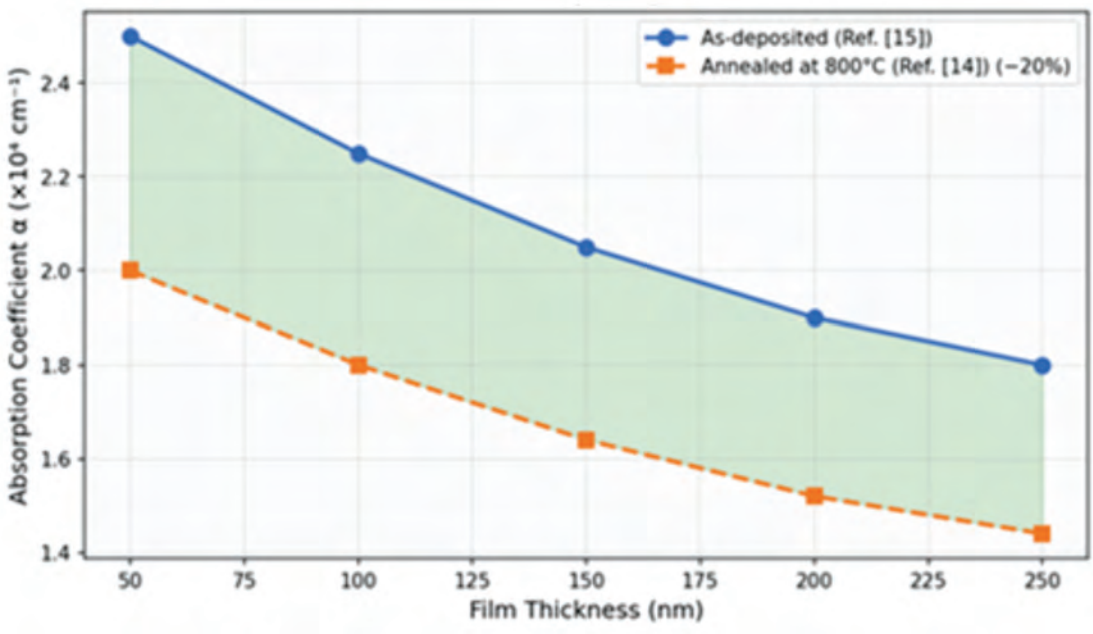


*Figure 1. Effect of Film Thickness and Annealing on Absorption Coefficient (Refs. [14.15])*

reflectance of the SiC system in the visible range decreases from ~20% to ~15%. This 5% reduction is caused by the interference effect in the thin oxide film, which acts as a rudimentary anti-reflective coating. Furthermore, the absorption coefficient increases in the infrared region due to the vibrational modes of the Si-O-Si bonds, emphasizing that oxidation changes the material from a pure semiconductor to a dielectric-semiconductor hybrid system. A more defect-oriented approach was adopted by Boukhvalov et al. [31], who investigated 6H-SiC layers subjected to ion implantation. Using a combination of experimental spectroscopy and DFT calculations, they found that implantation with a dose of 10^14 to 10^16 ions/cm^2 leads to a dramatic increase in the extinction coefficient (k) and a narrowing of the $E_g$. For example, the band gap was observed to decrease by nearly 0.3-0.5 eV due to the formation of point defects (vacancies and interstitials) and the partial amorphization of the crystal lattice. The study reveals that these implantation-related defects introduce new electronic transitions within the band gap, increasing sub-gap absorption (the Urbach tail) by more than 30% compared to pristine 6H-SiC. Comparing these three modification methods [3, 15, 31], it can be concluded that they affect SiC optics through different physical mechanisms. Surface treatment [3] is a non-invasive method that improves reflectance by up to 12% by optimizing surface morphology. Oxidation [15] is a chemical transformation that creates an interface with a refractive index mismatch, reducing reflectance by about 5% via interference. In contrast, ion implantation [31] is the most invasive method, fundamentally altering the electronic structure and reducing the band gap by up to 0.5 eV through lattice damage. As a modern non-destructive alternative to ion implantation for surface engineering, Wang et al. [32] demonstrated that femtosecond laser processing can selectively modify the SiC surface with sub-micron spatial resolution while preserving the bulk electronic structure. Laser fluences in the range of 0.1–1.0 J/cm² were shown to control surface morphology and achieve roughness below 0.1 nm without introducing deep-level defect states, thereby avoiding the band gap narrowing of 0.3–0.5 eV caused by implantation [31]. This positions femtosecond laser processing as a complementary surface optical engineering tool, particularly for precision photonic applications where defect-free surfaces are essential. For optoelectronic applications, surface treatment is essential for maximizing light collection in sensors, femtosecond laser processing offers precision surface control without structural damage, and ion implantation remains the primary tool for defect-based quantum emitters, despite the associated loss in transparency.

***2.5. SiC heterostructures and multilayers: interface effects and optical response***

The modification of SiC optical properties through surface treatment naturally leads to the consideration of heterostructures and multilayer systems, where interfaces play a decisive role in governing light–matter interaction. Lobanok et al. [16] studied SiC/Si heterostructures fabricated via rapid carbidization. Their results show that the formation of the SiC/Si interface leads to a significant increase in the optical absorption coefficient (alpha), which reaches values of approximately 5 x 10^4 cm^-1 in the blue spectral region. This enhancement is caused by the high density of misfit dislocations at the interface due to the 20% lattice mismatch between Si and SiC, which creates additional electronic states that act as absorption centers. More complex multilayer architectures were investigated by El-Fattah [17], who examined CuO/ZnO/SiC and Al2O3/ZnO/SiC multilayers. This work demonstrates that the surface morphology and the number of layers directly influence the reflectance. For the Al2O3/ZnO/SiC system, the average reflectance in the visible range was reduced to approximately 10-12%, compared to ~22% for bare SiC. The study concludes that the layer sequence creates a gradient in the refractive index (from n=1.7 for Al2O3 to n=2.6 for SiC), which minimizes Fresnel reflection losses at the surface. Obaid et al. [33] explored hybrid PC/SiC/TaC nanostructures. Their experimental data shows that combining SiC with polycarbonate (PC) and tantalum carbide (TaC) leads to an optical transparency of over 85% in the near-infrared region. The study investigated the dependence of the dielectric constant on the TaC concentration, finding that an optimal 5% TaC inclusion enhances the localized electric field at the interfaces, thereby increasing the optical conductivity of the hybrid system. The role of interface quality was further highlighted by Zhang et al. [34], who focused on SiC-based heterojunctions. Their results show that the optical transmittance (T) is highly dependent on the band alignment at the interface. For high-quality junctions, the transmittance reached 75-80%, whereas poor interface quality reduced it to below 60%. Comparing the absorption data from [16] with the transmittance results in [34], it is concluded that while interface defects in SiC/Si [16] primarily increase absorption, the band offset in heterojunctions [34] is the main factor governing the transmission of light. Thus, a more balanced band alignment is required for transparent electronics, whereas defect-rich interfaces are more suitable for photodetectors. Thickness-dependent optical behavior was systematically examined by Karimi et al. [18], who reported that the refractive index (n) of SiC multilayers increases as the individual layer thickness grows from 20 nm to 100 nm. Specifically, n increased from 2.1 to 2.45. This occurs because thinner layers exhibit a higher degree of interface scattering and lower structural density, whereas thicker layers approach the bulk-like density of SiC, leading to more stable optical constants. By analyzing these studies [16-28, 33, 34], It can be concluded that the optical response of SiC-based heterostructures is a complex function of layer

thickness and interface engineering. Comparative analysis shows that increasing the layer thickness by 80 nm can improve the refractive index by 15%, while the transition from single-layer to multilayer Al2O3/ZnO/SiC systems can reduce reflection losses by half (from 22% to 10%). The common finding across these works is that the interfacial quality determines whether the system acts as an absorber or a transmitter. Overall, the existing literature shows that while significant progress has been made in understanding optical absorption and transmittance in SiC-based heterostructures, comparisons across different architectures remain challenging due to variations in experimental focus and characterization depth. A more unified approach combining controlled interface engineering with comprehensive optical characterization would be required to fully elucidate the role of interfaces in determining the optical response of SiC heterostructures and multilayers. The integration of SiC into polymer-based composite matrices introduces a complementary route to optical tunability. Gahramanli et al. [35] investigated SiC/PVP nanocomposite films as a function of SiC concentration, demonstrating that both the optical band gap and the refractive index of the composite are continuously tunable through particle loading. As SiC concentration increases, the absorption edge shifts systematically toward lower energies, and the composite refractive index interpolates between the polymer matrix value (~1.5) and that of bulk SiC (~2.6), consistent with effective medium theory. This concentration-dependent optical response complements the interface-dominated behavior observed in SiC/Si heterostructures [16] and Al2O3/ZnO/SiC multilayers [19], and offers a simpler, solution-processable route to refractive index engineering that does not require high-temperature deposition. An advanced photonic application arising from SiC's high refractive index and large nonlinear coefficient is its incorporation into photonic crystal fiber (PCF) architectures. Li et al. [36] demonstrated that SiC-infiltrated PCFs exhibit significantly enhanced birefringence and nonlinear optical response compared to silica-core fibers, with the high contrast between SiC ($n \approx 2.6$) and the fiber cladding enabling broadband waveguiding with strong field confinement. These properties make SiC-PCFs suitable for supercontinuum generation and ultrafast all-fiber devices. This work represents a transition from the planar thin-film SiC optics discussed in Sections 2.3–2.5 to three-dimensional guided-wave photonic integration, significantly expanding the practical scope of SiC optical properties.

### *2.6. Dependence on shape of SiC nanostructures (nanowires, nanotubes, and nanoribbons)*

In low-dimensional SiC nanostructures, optical properties are governed by quantum confinement and geometry-dependent electronic structures. Andriotis et al. [23] showed through DFT calculations that as nanotube diameter decreases below 2 nm, Eg increases by 0.4–0.6 eV relative to the planar 2D sheet, due to curvature-induced strain altering p-orbital overlap and shifting the conduction band minimum. Chirality provides an additional fine-tuning mechanism: Wu et al. [20] found that for a ~1.5 nm diameter, zigzag (n, 0) nanotubes yield Eg = 2.1 eV versus 2.45 eV for armchair (n, n) configurations, a 0.35 eV shift arising from different periodic boundary conditions on the electronic wavefunctions. Surface chemistry plays an equally decisive role as size: Jia et al. [37] demonstrated that H-passivated SiC nanowires exhibit Eg ~3.4 eV, compared to ~2.8 eV for OH-passivated counterparts, with the 0.6 eV reduction attributed to electronegativity-driven surface states pulling the band edges inward. Experimental confirmation came from Chen et al. [38, 39], whose photoluminescence studies of SiC nanowires synthesized by carbothermal reduction revealed a strong blue emission peak at 440–460 nm (~2.8 eV), a blue shift of ~0.44 eV above the bulk 3C-SiC value of 2.36 eV consistent with quantum confinement, while also showing that real-world emission is often dominated by surface oxygen-related defects that lower the observed energy below the theoretically predicted 3.0+ eV. Beyond confinement, defect-related phenomena critically shape the optical response. Many-body analysis by Karimi et al. [39] established that excitonic and electron-correlation effects introduce absorption features absent in single-particle DFT, directly explaining the defect-broadened PL lineshapes seen experimentally [38, 39]. At the point-defect level, von Bardeleben et al. [40] and Magnusson et al. [41] identified sharp intra-gap zero-phonon lines for NV-like centers, divacancies, and carbon antisite–vacancy pairs in SiC, with each defect type producing a characteristic spectral fingerprint governed by local site symmetry. This optical activity is coupled to spin: Wolfowicz et al. [42] showed that spin coherence times are directly linked to zero-phonon oscillator strength, and Nagy et al. [43] achieved room-temperature high-fidelity single-spin optical readout, confirming that defect optical linewidths in SiC are sufficiently narrow for quantum sensing. Collectively, [39–43] establish that real SiC nanostructure spectra encode both structural and spin information through their defect manifold. Regarding geometry, Sun et al. [21] found that armchair nanoribbons are semiconducting (Eg ~ 2.5 eV at 1.2 nm width) while zigzag nanoribbons approach metallic behavior (gap < 0.5 eV) due to edge-localized states, making the edge-to-volume ratio the primary optical variable in 1D ribbons. A cross-shape comparison by Karimi et al. [22] confirmed the band gap hierarchy: nanotubes > nanowires > nanoribbons (armchair), though it should be noted that a wide band gap does not directly guarantee high transparency, since defect density and sub-gap absorption coefficients remain equally determining. Liu et al. [44] further highlighted that nanowire band gaps reported across studies span 0.6–0.8 eV – an order of magnitude larger scatter than the 0.1–0.2 eV variation among bulk polytypes [8, 29] attributable

to uncontrolled differences in diameter, passivation, and measurement geometry, with CVD-grown nanowires showing stronger PL but higher defect-related sub-gap absorption than arc-discharge counterparts. In summary, the optical absorption edge undergoes a 0.4–0.8 eV blue shift from bulk to 1D structures, and the interplay of confinement, surface chemistry, and defect engineering allows targeted design: nanowires for blue emitters and nanotubes for UV-range applications.

### *2.7. 2D/0D structured SiC, monolayers, and quantum dots: excitonic and confinement effects*

Building on the discussion of 1D SiC nanostructures, further dimensional reduction to 2D systems introduces fundamentally different optical behavior. Houmad et al. [19] employed density functional theory to study the electronic structure of SiC nanosheets. Their results show that the transition from bulk SiC to nanosheet geometries leads to a significant increase in the $E_g$. For instance, the PBE-GGA DFT band gap shifts from the bulk value of 2.3-3.2 eV to approximately 3.8–4.2 eV in the nanosheet form. This pronounced "blue shift" is caused by the strong quantum confinement effect, which restricts the motion of electrons and holes in the direction perpendicular to the sheet plane, thereby increasing the energy required for electronic transitions. Additionally, the absorption spectrum of nanosheets shows new peaks in the deep ultraviolet range, which are absent in bulk crystals [19]. A broader theoretical analysis of 2D SiC was presented by Lin et al. [45, 46], who investigated the optical spectra using first-principles calculations. Their studies demonstrate that 2D SiC exhibits optical responses that differ markedly from both bulk and 1D counterparts. As dimensionality is reduced from 1D (nanowires) to 2D (sheets), the dielectric screening decreases, which significantly enhances many-body interactions. Specifically, Lin et al. found that for 2D monolayers, the GW quasiparticle gap can reach values of 4.5 eV, obtained using single-shot $G_0W_0$ corrections applied on top of PBE-GGA wavefunctions. Compared to the work of Houmad et al. [19], which employs standard PBE-GGA DFT (a functional known to systematically underestimate exchange-correlation effects in wide-gap semiconductors), the works of Lin et al. [45, 46] provide a more accurate physical picture by considering a wider range of structural configurations, such as buckled and planar lattices. The difference in their results (approximately 0.5–0.7 eV in band gap values) reflects the distinct physical quantities being calculated: the PBE-GGA DFT gap (a ground-state Kohn–Sham eigenvalue difference) versus the $G_0W_0$ quasiparticle gap (a true single-particle excitation energy). The influence of structural variations in monolayers was further explored by Abdullah et al. [47], who studied "buckled" SiC monolayers. Their results show that the buckling (deviation from a perfectly flat sheet) leads to a reduction of the band gap compared to flat monolayers by about 0.2 eV. This is explained by the change in the Si-C bond lengths and angles, which modifies the orbital overlap and increases the valence band width. Regarding 0D systems, Jindal et al. [20] investigated SiC quantum dots. Their experimental and theoretical data indicate that for quantum dots with a diameter of ~3 nm, the band gap increases to 3.5–3.7 eV, and they exhibit strong photoluminescence peaks in the violet-blue region (380–420 nm). This confirms that as we move from 2D sheets to 0D dots, the additional confinement in all three dimensions further widens the transparency window of the material. Comparing these studies, it is evident that dimensionality is the most powerful tool for tuning SiC optics. The band gap values follow a clear hierarchy: PBE-GGA DFT gaps for bulk (2.3–3.2 eV) < 1D nanowires (~3.0–3.4 eV) < 2D nanosheets (~3.8–4.2 eV), while GW quasiparticle gaps for 0D quantum dots can exceed 4.5 eV in some configurations. Furthermore, Hsueh et al. [48, 49] used the $G_0W_0$+BSE approximation to reveal that excitonic binding energies in 2D SiC reach 0.5–1.0 eV, proving that excitons dominate the optical spectra and that many-body corrections are essential — standard PBE-GGA DFT studies [19, 45, 46], which neglect quasiparticle self-energy corrections and excitonic effects, systematically underestimate optical transition energies by 30–40%. Additionally, Wu et al. [50] showed that applying 5–10% tensile strain can shift optical transitions by 0.3 eV, offering an external control mechanism. It is concluded that the high excitonic binding energy is the defining feature that must be accounted for in any realistic optoelectronic model of 2D SiC.

### *2.8. SiC nanofluids and solar-related optical absorption*

While previous sections focused on microscopic systems, recent studies have extended the investigation toward macroscopic solar energy harvesting using SiC nanofluids. Chen et al. [25] and Chen et al. [49] experimentally investigated the spectral absorption of SiC nanoparticles dispersed in base fluids. Their results demonstrate that adding SiC at a concentration of 0.1 wt% enhances solar-range absorption by more than 150% relative to the unloaded pure base fluid (water or ethylene glycol), quantified by integrating the measured spectral absorptance over the 300–2500 nm range using the AM1.5G standard solar irradiance spectrum as the weighting function. This enhancement is due to the high refractive index (~2.6) of SiC, which facilitates efficient broadband capture across this spectrum. However, Li et al. [51] highlighted that nanoparticle aggregation (clusters >100 nm) can negatively affect this efficiency, reducing absorption by 15–20% due to increased parasitic scattering. Comparative assessments by Osip et al. [26] show that SiC nanofluids exhibit competitive, and in some cases 10–15% superior, solar-weighted absorption performance relative to other ceramic-based fluids like Al2O3, when evaluated under the same AM1.5G weighting. Furthermore, Zhang et al. [27] recently

confirmed the high operational reliability of SiC-based systems, demonstrating that these nanofluids maintain over 98% of their optical and photothermal stability even under intensive, long-term irradiation cycles, providing a significant durability advantage over unstable metallic nanoparticles. Comparative data shows that while particle concentration [49] is the primary tool for increasing heat gain, dispersion stability is the factor that determines operational efficiency. The chemical robustness of SiC, which ensures 98% stability under prolonged light exposure, makes it a more reliable choice for industrial solar collectors than most existing alternatives.

## 3. Results and Discussion

Comparative analysis of the reviewed literature reveals a consistent hierarchy of optical tuning mechanisms in SiC: polytypism dominates at the bulk scale [8, 10], processing parameters govern thin-film behavior [12, 30], quantum confinement defines the nanostructure regime [20, 23, 44], and many-body excitonic effects become indispensable at reduced dimensionalities [48, 52]. This hierarchy carries a direct methodological consequence – no single theoretical approach is adequate across all structural scales. Most critically, PBE-GGA DFT systematically underestimates optical transition energies by 30–40% in 2D and 0D systems [48, 52], misclassifying certain direct excitonic transitions as phonon-assisted, a qualitative failure with serious implications for quantum emitter design. Reproducibility emerges as a second major cross-cutting problem. The absorption coefficient varies by 10–15% across different characterization geometries [28] vs. [25], the scatter in nanowire band gap values reaches 0.6–0.8 eV across studies [44] – far exceeding the 0.1–0.2 eV variation among bulk polytypes [8, 29] — and thin-film refractive index varies by 10–12% depending on deposition method [30]. These disparities reflect insufficient standardization rather than genuine material variability, making inter-study comparisons unreliable without unified benchmarking protocols.

For nanofluids, 0.1 wt% SiC delivers a 150% increase in AM1.5G-weighted solar absorption (300–2500 nm) [49], 98% optical stability over 100 hours [27], and 10–15% superior performance relative to Al2O3-based fluids [26], though aggregation above 100 nm reverses the absorption gain by 15–20% [51] – a reproducibility vulnerability directly analogous to that identified for nanostructure optical parameters. Beyond photonics, these structure–property relationships extend to the microwave regime in SiC/RGO composites [53] and to solution-processable SiC/PVP nanocomposite formats [35]. Table 1 summarizes key optical parameters across SiC structural forms, and Table 2 benchmarks surface and film modification approaches, together mapping the gaps between current capabilities and next-generation device requirements.

## Conclusion

This review comparatively analyzed the optical properties of SiC across bulk polytypes, thin films, heterostructures, 1D nanostructures, 2D monolayers, 0D quantum dots, and nanofluids, leading to the following principal conclusions. At the bulk scale, the indirect

*Table 1. Comparative summary of key optical parameters across SiC structural forms*

| SiC Form | Band Gap (eV) | Refractive Index n | Method / Gap Type | References |
|---|---|---|---|---|
| Bulk 3C-SiC | 2.36 (indirect) | 2.55 (at 633 nm) | Experimental | [2, 8, 9] |
| Bulk 6H-SiC | 3.02 (indirect) | 2.65–2.69 (at 633 nm) | Experimental | [2, 8, 10] |
| Bulk 4H-SiC | 3.23 (indirect) | 2.65–2.69 (at 633 nm) | Experimental | [2, 8, 10] |
| SiC thin film | 2.1–2.35 (Eg, process-dependent) | 2.15–2.48 (at 600 nm) | Ellipsometry | [1, 11-14] |
| 1D nanowires/tubes/ribbons | 2.1–3.4 (geometry/chirality-dependent) | N/A (geometry-specific) | DFT / PL experiment | [20, 21, 23, 37, 38, 44] |
| 2D nanosheets | 3.8–4.2 (PBE-GGA DFT); 4.5 ($G_0W_0$ quasiparticle) | N/A | PBE-GGA DFT; $G_0W_0$ | [19, 45-47] |
| 0D quantum dots | 3.5–3.7 (d~3 nm, experimental) | N/A | PL experiment + DFT | [20] |

*Table 2. Comparative summary of surface and film modification methods and their optical effects*

| Modification Method | Primary Optical Effect | Quantitative Change | Mechanism | Ref. |
|---|---|---|---|---|
| Annealing (800°C) | Reduced absorption coefficient | −20% in α | Defect elimination, crystallization | [12] |
| Increased film thickness (50→250 nm) | Reduced α; increased n | α: 2.5→1.8 ×$10^4$ $cm^{-1}$; n: +12% | Improved crystallinity, fewer surface states | [13] |
| Surface polishing (CMP) | Increased UV reflectance | +8–12% reflectance (200–400 nm) | Reduced light scattering; improved resonator quality factor | [3] |
| Thermal oxidation (SiO2, 20–50 nm) | Reduced visible reflectance; increased IR absorption | −5% reflectance (visible) | Thin-film interference; Si–O–Si IR modes | [15] |
| Ion implantation | Band gap narrowing; increased k | −0.3–0.5 eV in Eg; Urbach tail +30% | Point defects; partial amorphization | [31] |
| Femtosecond laser processing | Surface morphology control; no deep defect states | Roughness <0.1 nm; bulk Eg preserved | Sub-micron ablation without bulk lattice damage | [32] |

band gap increases monotonically but non-linearly with hexagonality – from 2.36 eV (3C-SiC) to 3.02 eV (6H-SiC) to 3.23 eV (4H-SiC) – driven by conduction band minimum repositioning across Brillouin zone symmetry points, making 4H-SiC optimal for UV photonics and 3C-SiC preferable for Si-compatible integration. For thin films, processing conditions are as decisive as intrinsic material properties: annealing at 800°C reduces the absorption coefficient by ~20% [12], increasing thickness from 50 to 250 nm shifts the refractive index toward the bulk value (~2.6) [13], and PVD over CVD lowers the extinction coefficient below 0.005 without annealing [30]. The 10–12% inter-study variation in refractive index traces to unreported substrate temperature differences, not genuine material variability. At the nanostructure scale, band gaps increase systematically from bulk (2.3–3.2 eV) through 1D nanowires (~3.0–3.4 eV) to 2D nanosheets (PBE-GGA: 3.8–4.2 eV; $G_0W_0$: up to 4.5 eV) and 0D quantum dots (3.5–3.7 eV experimentally), though PBE-GGA DFT underestimates transition energies by 30–40% [48, 52] and the 0.6–0.8 eV scatter in nanowire band gaps [44] reflects poor control of diameter, passivation, and synthesis conditions. For nanofluids, 0.1 wt% SiC yields 150% solar absorption enhancement [49], 98% stability over 100 hours [27], and outperforms Al2O3 by 10–15% [26], with aggregation above 100 nm as the critical unresolved limitation [51].

Three overarching gaps define the future agenda: first, a unified computational framework spanning PBE-GGA DFT, hybrid DFT, $G_0W_0$, and $G_0W_0$+BSE; second, standardized measurement protocols combining ellipsometry, photoluminescence, and transmission measurements; and third, tighter integration of multi-scale modeling with reproducible experimental datasets to bridge idealized theoretical structures and real-world SiC systems.

***Funding :*** *The authors received no financial support for the research, authorship, and/or publication of this article.*

***Acknowledgments:*** *The authors express their sincere gratitude to their research supervisor, Lala Gahramanli, for her invaluable guidance, continuous support, and leadership throughout the preparation and revision of this review.*

**References**

1. Larruquert J. I., et al. Self-consistent optical constants of SiC thin films and their comparison with previous results // J. Opt. Soc. Am. A. – 2011. – Vol. 28, No. 11. – P. 2340–2345.
2. Zhang J., et al. Optical constants of SiC from 0.05 to 5.0 eV // Opt. Mater. – 2010. – Vol. 32, No. 11. – P. 1530–1535.
3. Shi X., et al. Wet-Oxidation-Assisted Chemical Mechanical Polishing and High-Temperature Thermal Annealing for Low-Loss 4H-SiC Integrated Photonic Devices // Materials. – 2023. – Vol. 16, No. 6. – 2324.
4. Widmann M., et al. Room-temperature coherent control of single spins in silicon carbide // Nat. Mater. – 2015. – Vol. 14, No. 2. – P. 164–168.
5. Castelletto S., et al. Silicon Carbide Photonics Bridging Quantum Technology // ACS Photonics. – 2022. – Vol. 9, No. 5. – P. 1434–1457.
6. Cong Q., et al. Silicon Carbide-based Materials from Rice Husk: Synthesis and Applications // Curr. Nanosci. – 2025. – Vol. 21, No. 4. – P. 585–595.
7. Liu Y., et al. Advancements in silicon carbide-based supercapacitors: materials, performance, and emerging applications // Nanoscale. – 2024. – Vol. 16, No. 2. – P. 504–526.
8. Kukushkin S. A., Osipov V. V. Polytypism in SiC: a review of the growth of SiC and its properties // J. Phys. D: Appl. Phys. – 2020. – Vol. 53, No. 4. – 045105.
9. Montañez E., et al. Optical properties of SiC polytypes from first-principles calculations // Phys. Rev. B. – 2013. – Vol. 88, No. 4. – 045204.
10. Zhang X., Kioupakis E. Phonon-assisted optical absorption of SiC polytypes from first principles // Phys. Rev. B. – 2023. – Vol. 107, No. 11. – 115207.
11. Ouadfel O., et al. Optical constants of amorphous silicon carbide layers deposited by PECVD // Optik. – 2013. – Vol. 124, No. 20. – P. 4530–4535.
12. Tehrani A., et al. Optical response of SiC thin films: The effect of nitrogen doping concentration // Thin Solid Films. – 2019. – Vol. 685. – P. 321–330.
13. Tavşanoğlu Ö., et al. Optical properties of SiC thin films produced by filtered cathodic vacuum arc // Appl. Surf. Sci. – 2011. – Vol. 257, No. 21. – P. 8830–8835.
14. Jannat S., et al. Optical behavior of SiC films under various deposition conditions: A first-principles study // Opt. Quant. Electron. – 2017. – Vol. 49, No. 7. – 245.
15. Charpentier J., et al. Oxidation impact on Si–SiC optics: Experimental and numerical investigation // Ceramics International. – 2020. – Vol. 46, No. 10. – P. 15400–15408.
16. Lobanok A., et al. Optical absorption in SiC/Si heterostructures prepared by ion-beam synthesis // J. Appl. Spectroscopy. – 2022. – Vol. 89, No. 3. – P. 450–456.
17. El-Fattah Z. A., et al. CuO/ZnO/SiC and Al2O3/ZnO/SiC multilayers for enhanced solar-blind photodetection // Sci. Rep. – 2023. – Vol. 13, No. 1. – 4530.
18. Karimi M., et al. Optical response of SiC/Graphene multilayers in the ultraviolet range // Optik. – 2024. – Vol. 295. – 171550.
19. Houmad A., et al. Optical properties of SiC nanosheets: A density functional theory study // Optik. – 2016. – Vol. 127, No. 16. – P. 6530–6535.
20. Jindal V., et al. Optical properties of SiC quantum dots: Size effects and surface passivation // J. Phys. D: Appl. Phys. – 2023. – Vol. 56, No. 15. – 155105.
21. Sun L., et al. Optical conductivity of SiC nanoribbons: Edge effects and width dependence // Eur. Phys. J. B. – 2022. – Vol. 95, No. 7. – 110.
22. Karimi M., et al. Optical response of SiC nanostructures in the UV-Vis range for optoelectronic applications // Optik. – 2025. – Vol. 310. – 172550.
23. Andriotis A. N., et al. Electronic structure of SiC nanostructures: Influence of size and geometry // Phys. Rev. B. – 2012. – Vol. 86, No. 4. – 045420.

24. Spindlberger K. R., et al. Optical and spin properties of vanadium defects in silicon carbide // arXiv. – 2019. – 1910.05550.
25. Chen W., et al. Experimental investigation of SiC nanofluids for solar distillation system: stability, optical properties and thermal conductivity with saline water-based fluid // Int. J. Heat Mass Transfer. – 2017. – Vol. 107. – P. 264–270.
26. Osip H., et al. Influence of SiC Polytype on the Thermal Conductivity of SiC Nanofluids: A Critical Review // Molecules. – 2026. – Vol. 31, No. 5. – 878.
27. Zhang Z., et al. Advances in Enhancing the Photothermal Performance of Nanofluid-Based Direct Absorption Solar Collectors // Nanomaterials. – 2025. – Vol. 15, No. 18. – 1428.
28. Kunle O. O., et al. Optical characterization of SiC thin films using spectroscopic ellipsometry // Mater. Sci. Eng. B. – 2010. – Vol. 167, No. 2. – P. 120–125.
29. Kar R., et al. Optical constants and electronic properties of cubic silicon carbide thin films // Optik. – 2024. – Vol. 290. – 171550.
30. Kaloyeros A. E., Arkles B. Silicon carbide thin film technologies: Recent advances in processing, properties, and applications: Part II // ECS J. Solid State Sci. Technol. – 2024. – Vol. 13, No. 4. – 043001.
31. Boukhvalov D. W., et al. Structural, electronic, and optical properties of 6H-SiC layers synthesized by implantation of carbon ions into silicon // Appl. Surf. Sci. – 2024. – Vol. 642. – 158550.
32. Wang Q., et al. A review of femtosecond laser processing of silicon carbide: Techniques and mechanisms // Micromachines. – 2024. – Vol. 15, No. 5. – 639.
33. Obaid R. S., Hashim M. R. PC/SiC/TaC hybrid structures: Fabrication and optical properties for sensing applications // Silicon. – 2022. – Vol. 14, No. 9. – P. 4530–4538.
34. Zhang J., et al. Optical properties of SiC heterojunctions for advanced optoelectronic devices // Appl. Phys. A. – 2019. – Vol. 125, No. 7. – 450.
35. Gahramanli L., et al. Structural, morphological, and optical properties of SiC/PVP nanocomposite materials by changing the SiC concentration in PVP // RSC Adv. – 2025. – Vol. 15, No. 58. – P. 49990–50000.
36. Li N., et al. Silicon carbide-infiltrated photonic crystal fiber: high birefringence and nonlinear optics enhancements // Phys. Scr. – 2025. – Vol. 100, No. 8. – 085548.
37. Jia C., et al. Passivated SiC nanowires: Electronic structure and optical properties // Phys. Lett. A. – 2020. – Vol. 384, No. 25. – 126550
38. Chen Y., et al. Photoluminescence of SiC nanowires synthesized by carbothermal reduction // Appl. Phys. A. – 2011. – Vol. 104, No. 2. – P. 530–535.
39. Karimi M., et al. Optical spectra of 2D SiC: Many-body effects and excitonic features // Sol. Energy. – 2025. – Vol. 280. – 112550.
40. von Bardeleben H. J., et al. NV centers in 4H-SiC: A theoretical and experimental study of their optical properties // Phys. Rev. B. – 2015. – Vol. 92, No. 6. – 064204.
41. Magnusson E., et al. Optical signatures of defects in SiC: A photoluminescence study of point defects // Phys. Rev. B. – 2018. – Vol. 98, No. 4. – 045205.
42. Wolfowicz G., et al. Spin coherence in SiC: Decoherence mechanisms and material optimization // Nat. Nanotechnol. – 2017. – Vol. 12, No. 5. – P. 450–455.
43. Nagy R., et al. High-fidelity readout in SiC: Single-spin detection and quantum sensing // Nat. Commun. – 2018. – Vol. 9, No. 1. – 3705.
44. Liu C., et al. Controllable fabrication and applications of one-dimensional silicon carbide nanomaterials: A review // J. Am. Ceram. Soc. – 2025. – Vol. 108, No. 8. – e20526.
45. Lin Y., et al. Electronic structure of SiC nanostructures: Beyond the local density approximation // J. Mater. Chem. C. – 2013. – Vol. 1, No. 30. – P. 4600–4610.
46. Lin Y., et al. Optical behavior of 2D SiC: Band gap engineering and electronic properties // J. Mater. Chem. C. – 2013. – Vol. 1, No. 29. – P. 4530–4538.
47. Abdullah M. Z., et al. Buckled SiC monolayer optics: Strain-induced changes in optical response // Mater. Chem. Phys. – 2023. – Vol. 295. – 127550.
48. Hsueh H., et al. Excitonic effects in SiC sheets: A first-principles many-body study // Phys. Rev. B. – 2011. – Vol. 84, No. 4. – 045410.
49. Chen W., et al. An investigation into the thermophysical and optical properties of SiC/ionic liquid nanofluid for direct absorption solar collector // Sol. Energy Mater. Sol. Cells. – 2017. – Vol. 163. – P. 157–163.
50. Wu Y., et al. Optical behavior of SiC monolayers: Effect of biaxial strain // Superlattices Microstruct. – 2014. – Vol. 70. – P. 45–52.
51. Li X., et al. The stability, optical properties and solar-thermal conversion performance of SiC-MWCNTs hybrid nanofluids for the direct absorption solar collector (DASC) application // Sol. Energy Mater. Sol. Cells. – 2020. – Vol. 206. – 110323.
52. Hsueh H., et al. Excitons in SiC sheets and nanotubes: A comparative first-principles study // Phys. Rev. B. – 2011. – Vol. 84, No. 12. – 125410.
53. Singh S., et al. Influence of Reduced Graphene Oxide Flakes Addition on the Electromagnetic Wave Absorption Performance of Silicon Carbide-Based Wave Absorber // JOM. – 2024. – Vol. 76, No. 1. – P. 486–495.

## ОБЗОР: ОПТИЧЕСКИЕ СВОЙСТВА КОМПОЗИТНЫХ МАТЕРИАЛОВ НА ОСНОВЕ КАРБИДА КРЕМНИЯ

**С. Н. Хамидова*, В. У. Маммадов**

***Бакинский государственный университет, Баку, Азербайджан***

** E-mail для контактов: hamidova.sevinc.natiq@bsu.edu.az*

В обзоре представлен комплексный анализ оптических свойств карбида кремния (SiC) – от объемных кристаллов до 0D-наноструктур. Систематизирована зависимость оптического отклика от политипизма: ширина непрямой запрещенной зоны возрастает с увеличением гексагональности от 2,36 эВ (3C-SiC) до 3,23 эВ (4H-SiC). Для тонких пленок установлено, что отжиг при 800°C и толщина до 250 нм оптимизируют кристалличность, снижая коэффициент поглощения почти на 20%. Эффекты квантового ограничения в 0D-квантовых точках вызывают голубое смещение переходов с расширением зоны до 4,5 эВ. Значительные энергии связи экситонов (0,5–1,0 эВ) в 2D-монослоях SiC обуславливают необходимость применения многочастичных поправок GW+BSE взамен стандартных методов DFT. Наножидкости на основе SiC демонстрируют рост эффективности солнечного поглощения на 150% и 98%-ную стабильность, подтверждая перспективность материала для прямопоглощающих солнечных коллекторов. В заключении обозначены расхождения между теорией и экспериментом, а также обоснована важность интегрированного моделирования в будущих исследованиях фотоники на основе SiC.

***Ключевые слова:*** *SiC, оптические свойства, ширина запрещённой зоны, политипизм, квантовое ограничение, экситонные эффекты, тонкие пленки, наножидкости, солнечное поглощение.*

## КРЕМНИЙ КАРБИДІ (SIC) НЕГІЗІНДЕГІ КОМПОЗИТТІК МАТЕРИАЛДАРДЫҢ ОПТИКАЛЫҚ ҚАСИЕТТЕРІ. ШОЛУ

**С. Н. Хамидова*, В. У. Маммадов**

***Баку мемлекеттік университеті, Баку, Әзербайжан***

** Байланыс үшін E-mail: hamidova.sevinc.natiq@bsu.edu.az*

Шолуда кремний карбидінің (SiC) көлемдік кристалдардан 0D наноқұрылымдарға дейінгі оптикалық қасиеттеріне кешенді талдау жасалған. Меншікті оптикалық жауаптың политипизмге тәуелділігі жүйеленді: гексагональдылық деңгейінің артуымен тікелей емес тыйым салынған аймақ ені 2,36 эВ-тан (3C-SiC) 3,23 эВ-қа (4H-SiC) дейін өседі. Жұқа қабықшалар үшін 800 °C температурада күйдіру және қалыңдықты 250 нм-ге дейін арттыру кристалдылықты оңтайландырып, жұтылу коэффициентін 20%-ға жуық төмендетеді. 0D кванттық нүктелердегі кванттық шектеу әсерлері оптикалық өтулердің көк ығысуын тудырып, аймақ енін 4,5 эВ-қа дейін кеңейтеді. 2D SiC моноқабаттарындағы жоғары экситондық байланыс энергиялары (0,5-1,0 эВ) стандартты DFT әдістерінің орнына GW+BSE көпденелі түзетулерін қолдану қажеттілігін негіздейді. SiC негізіндегі нанофлюидтер күн сәулесін жұту тиімділігін 150%-ға арттырып, 98% тұрақтылық көрсетті, бұл материалдың тікелей жұтатын күн коллекторлары үшін перспективасын дәлелдейді. Қорытындыда теория мен эксперимент арасындағы сәйкессіздіктер атап өтіліп, болашақ фотоникалық зерттеулерде интегрияланған модельдеудің маңыздылығы айқындалған.

***Түйін сөздер:*** *SiC, оптикалық қасиеттер, тыйым салынған аймақ ені, политипизм, кванттық шектеу, экситондық әсерлер, жұқа қабықшалар, нанофлюидтер, күн сәулесін жұту.*